PHYSICAL REVIEW B **92**, 100405(R) (2015)

Domain walls within domain walls in wide ferromagnetic strips

Touko Herranen* and Lasse Laurson
COMP Centre of Excellence and Helsinki Institute of Physics, Department of Applied Physics, Aalto University, P.O. Box 11100, FI-00076 Aalto, Espoo, Finland
(Received 17 June 2015; published 16 September 2015)

We carry out large-scale micromagnetic simulations that demonstrate that due to topological constraints, internal domain walls (Bloch lines) within extended domain walls are more robust than domain walls in nanowires. Thus, the possibility of spintronics applications based on their motion channeled along domain walls emerges. Internal domain walls are nucleated within domain walls in perpendicularly magnetized media concurrent with a Walker breakdown-like abrupt reduction of the domain wall velocity above a threshold driving force, and may also be generated within pinned, localized domain walls. We observe fast field and current driven internal domain wall dynamics without a Walker breakdown along pinned domain walls, originating from topological protection of the internal domain wall structure due to the surrounding out-of-plane domains.

DOI: 10.1103/PhysRevB.92.100405 PACS number(s): 75.60.Ch, 75.78.Fg, 75.78.Cd

During recent years, a lot of effort has been devoted to understanding properties of magnetic domain walls (DWs) and their dynamics. A major driving force behind these studies is the emergence of next generation ICT components based on DWs, such as memory devices [1,2] and logic gates [3]. At the same time, magnetic DWs constitute a suitable playground to study several key fundamental physics ideas and concepts, ranging from topology [4] to nonequilibrium critical phenomena [5,6].

In general, DWs may have various internal degrees of freedom [7], which are essential for their magnetic field or spin-polarized current-driven dynamics, and have recently been shown to be useful, e.g., for channeling spin waves along extended DWs [8]. In narrow ferromagnetic (nano)strips [both in soft Permalloy strips and strips with a high perpendicular magnetic anisotropy (PMA)], the Walker breakdown [9], or the onset of precession of the DW internal magnetization $\mathbf{m}^{\mathrm{DW}}$, leads to an abrupt decrease of the DW propagation velocity above the Walker field B_{W} or current density j_{W} [10–12]. Such behavior is captured also by simple one-dimensional (1D) models [12] of DWs in nanowires and strips.

In wider PMA strips with longer DWs (where the 1D models are no longer applicable), one may expect that a Walker breakdown-like abrupt reduction of the DW propagation velocity still takes place, but that the related excitation(s) of $\mathbf{m}^{\mathrm{DW}}$ can no longer be spatially uniform [13]. Possible origins for the symmetry breaking leading to incoherent precession of $\mathbf{m}^{\mathrm{DW}}$ in different parts of the DW could be edge effects, and/or quenched disorder, interacting with the DW [10,14–20]; these may include dislocations, precipitates, grain boundaries, thickness fluctuations of the strip, etc. Here we explore the dynamics of extended DWs in wide CoPtCr PMA strips, with a Bloch wall equilibrium structure, using large-scale micromagnetic simulations with and without quenched disorder. We show that in wide enough strips and for driving forces exceeding a threshold value (B_{W} or j_{W}), the internal degrees of freedom of the DW are indeed excited inhomogeneously along the DW. These nonuniformities can be well-described as a set of internal DWs (IDWs), similar to Bloch lines observed, e.g., in the context of bubble domains in garnet films [21–25], separating in-plane domains within the main DW; see Fig. 1(d). Such IDWs, which resemble transverse DWs [26] found in narrow nanostrips with in-plane magnetization [27–29], can also be nucleated within DWs pinned by notches, and subsequently driven along the localized main DW by magnetic fields or spin-polarized currents. We compute the driving force dependence of the velocity of the various IDW types observed, and find that they do not experience a Walker breakdown, due to topological constraints originating from the out-of-plane domains surrounding the IDWs. Thus, the possibility to use extended DWs as channels for fast IDW propagation emerges, with potential applications in spintronics.

The micromagnetic simulations are performed using the GPU-accelerated micromagnetic code MuMax3 [30–32], solving the Landau-Lifshitz-Gilbert equation [33,34],

$$\partial \mathbf{m}/\partial t = \gamma \mathbf{H}_{\mathrm{eff}} \times \mathbf{m} + \alpha \mathbf{m} \times \partial \mathbf{m}/\partial t, \qquad (1)$$

where $\mathbf{m}$ is the magnetization, γ the gyromagnetic ratio, and $\mathbf{H}_{\mathrm{eff}}$ the effective field, with contributions due to exchange, Zeeman, and demagnetizing energies. We consider CoPtCr strips of thickness $L_z = 20$ nm [35], and widths L_y ranging from 150 nm to 3 μm, with the saturation magnetization $M_{\mathrm{s}} = 3 \times 10^5$ A/m, exchange constant $A = 10^{-11}$ J/m, and the damping parameter $\alpha = 0.2$. The first-order uniaxial anisotropy constant $K_{\mathrm{u}} = 2 \times 10^5$ J/m^3, and an out-of-plane easy axis is considered, to take into account the PMA nature of the strip [36]. The discretization cells have dimensions of $\Delta_x = \Delta_y = 3$ nm, and $\Delta_z = 20$ nm; we chose to use only one layer of computational cells in the z direction, since a finer discretization in that direction did not change the results.

We start by considering the field-driven dynamics of DWs in perfect CoPtCr strips, with two out-of-plane domains separated by a Bloch DW with the internal magnetization $\mathbf{m}^{\mathrm{DW}} = +M_{\mathrm{s}}\hat{y}$ as an initial state. We employ a simulation window of length $L_x = 6\,\mu$m centered around and moving with the DW. When driven with a field of magnitude $B_{\mathrm{ext}} < B_{\mathrm{W}}(L_y)$ along z, we observe a slight, B_{ext}-dependent tilting of the propagating DW; see Figs. 1(a) and 1(c): as $B_{\mathrm{ext}}\hat{z}$ rotates $\mathbf{m}^{\mathrm{DW}}$

*touko.herranen@aalto.fi

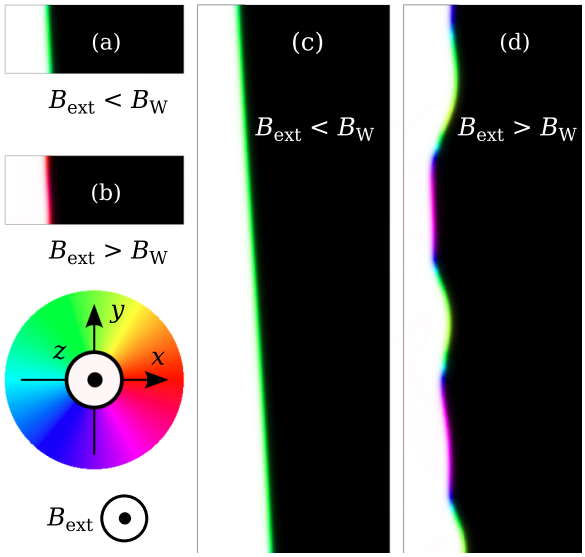

FIG. 1. (Color online) Snapshots of field-driven DWs in perfect CoPtCr strips with B_{ext} along z. (a) For a narrow strip ($L_y = 150$ nm), the DW is a Bloch DW with $\mathbf{m}^{DW}$ roughly along y for $B_{ext} < B_W$, while (b) for $B_{ext} > B_W$, $\mathbf{m}^{DW}$ oscillates between spatially almost uniform configurations. (c) For a wider strip ($L_y = 1.2$ μm), $\mathbf{m}^{DW}$ is uniform for $B_{ext} < B_W$, but (d) breaks into a dynamic pattern of in-plane domains separated by IDWs for $B_{ext} > B_W$.

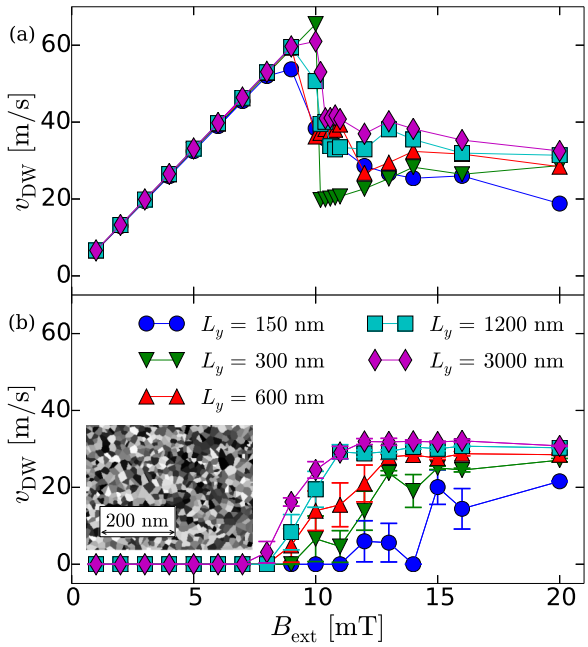

FIG. 2. (Color online) The average DW velocity v_{DW} as a function of B_{ext} (applied along the $+z$ direction) in CoPtCr strips of different widths L_y, in (a) perfect strips and (b) strips with a random 7% standard deviation variation of the anisotropy strength K_u in each grain; an example of the grain structure is shown in the inset. Notice the strong size effect in the depinning field in (b).

away from the y direction, the DW tries to align itself with its $\mathbf{m}^{DW}$, to minimize stray fields. Notice that this effect arises here without the Dzyaloshinskii-Moriya interaction [37], and that the sign of B_{ext} controls the tilt direction. For $B_{ext} > B_W$, the DW dynamics depends strongly on the strip width: for narrow strips [see Fig. 1(b)], $\mathbf{m}^{DW}$ oscillates between spatially almost uniform configurations, while for wider strips with longer DWs, $\mathbf{m}^{DW}$ breaks into a dynamic, spatially nonuniform pattern, initially nucleated from the sample edges; snapshots of the magnetization configurations [Fig. 1(d)] reveal that $\mathbf{m}^{DW}$ is broken into a set of in-plane domains, separated by IDWs (Bloch lines). These patterns are highly dynamic, with different parts of the DW either ahead or behind the average DW position. The IDWs move along the narrow (width ~9 nm) main DW, with annihilation and nucleation events of pairs of IDWs taking place repeatedly [38]; an example animation of this complex process is provided as Supplemental Material [39].

Figure 2(a) shows the steady state DW velocity v_{DW} as a function of B_{ext} for perfect strips of different widths L_y. For all L_y values considered, v_{DW} exhibits the same linear dependence on B_{ext} for $B_{ext} < B_W(L_y)$, with $B_W(L_y)$ in the range 9–10 mT; above B_W, v_{DW} is smaller than its (local) maximum obtained for smaller fields (indeed, a reduction of v_{DW} by a factor of α^2 is expected in the presence of many Bloch lines [23–25]), and displays a relatively complex depedence on B_{ext}, originating from the incoherent dynamics of $\mathbf{m}^{DW}$ at different parts of the DW. Also, current-driven DW dynamics (not shown) exhibits a velocity drop and IDWs nucleated above j_W [40].

In order to account for the effect of quenched disorder, here assumed to originate from the polycrystalline structure of the strip [41], we construct grains using a Voronoi tessellation [14,15], with an average grain size of 11.9 nm [35]; see the inset of Fig. 2. For each grain i, we assign a different, Gaussian distributed random anisotropy strength $K_{u,i}$, with mean K_u and standard deviation $\sigma = 0.07K_u$. Here, we consider with $L_x = 6$ μm. The DW is initialized at $x = -1.5$ μm, with the origin being in the middle of the sample. The disorder results in a finite, σ-dependent depinning field, as evidenced by Fig. 2(b), where averages over 5 disorder realizations are presented. Notice the strong size effect in the depinning field, with the longer DWs depinning for smaller B_{ext}. For longer DWs, $\mathbf{m}^{DW}$ now precesses nonuniformly for all B_{ext} values with $v_{DW} > 0$, including those below B_W of the corresponding perfect system; thus, the nonuniform internal degrees of freedom of the DW can also be induced by strong enough disorder, in addition to the sample edges. A possible interpretation of this is a spatially fluctuating B_W due to the different anisotropies in different grains.

IDWs can also be created within localized, pinned main DWs; such setups could be useful to experimentally test our results. We consider here DWs pinned by triangular notches (with 50-nm-long sides, and a $50\sqrt{2} \approx 70.7$-nm-long base) in strips of width $L_y = 1.2$ μm and length $L_x = 6$ μm, with disorder $\sigma = 0.1K_u$. By applying a 5-ns-long square field pulse of amplitude $B_{ext} = \pm 20$ mT (i.e., above B_W) along z, the pinned DW bends as its central part propagates, and $\mathbf{m}^{DW}$ exhibits spatially nonuniform dynamics (as $B_{ext} > B_W$); see Fig. 3. After the pulse, the curved DW gets pinned by disorder and may contain long-lived pinned nonuniformities in its $\mathbf{m}^{DW}$: stable 180° IDWs (Bloch lines) within the pinned main DW are formed with a roughly 40% success rate (estimated from

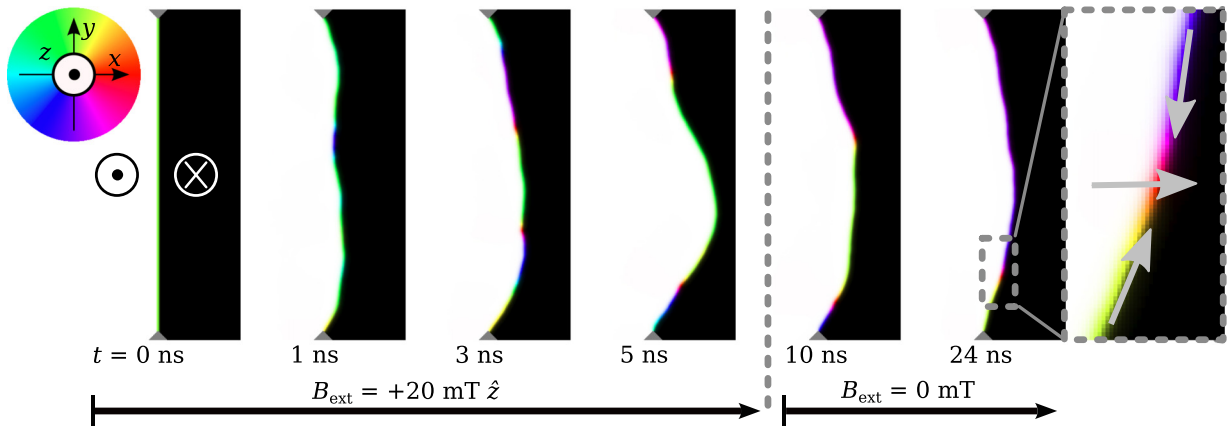

FIG. 3. (Color online) IDWs may be generated within pinned DWs in disordered CoPtCr strips by field pulses. A field pulse of magnitude $B_{\rm ext} = 20$ mT $> B_{\rm W}$ and duration of 5 ns, followed by relaxation in zero field, results in one pinned IDW, shown magnified in the last frame. The gray arrows indicate the direction of the in-plane DW magnetization around the IDW.

an ensemble of 100 disorder realisations). Also 360° IDWs are sometimes observed. Figure 3 shows a typical example of the process, with the end result of one head-to-head (H2H) 180° IDW, pinned by the disorder even after the relaxation time of 19 ns in zero field; the same process is also showed in a Supplemental Material movie [39]. Magnification of the IDW magnetization (last frame of Fig. 3) reveals that the IDW resembles transverse DWs in narrow in-plane systems (e.g., Permalloy nanostrips) [26–28]; we estimate the IDW width along the main DW to be 30 nm. While the random disorder induces a stochastic IDW nucleation process, the properties (direction $\pm z$, etc.) of the field pulse still affect the polarity of the IDWs created; $B_{\rm ext} > 0$ tends to lead to IDWs with $m_x^{\rm IDW} > 0$ (as, e.g., in Fig. 3), whereas $B_{\rm ext} < 0$ gives mostly rise to IDWs with $m_x^{\rm IDW} < 0$; for both polarities, the IDW may have either a H2H or tail-to-tail (T2T) configuration.

Examples of these four IDW configurations are presented in Fig. 4. Due to the geometry shown in Fig. 4, the IDWs can be driven by fields along $\pm y$ directions. To study the velocity-field characteristics of the IDWs, we first move all of them from their random initial positions to close to the lower edge of the strip by applying field pulses of a small magnitude. Then, a driving field $B_{\rm ext}$ is applied along $+y$ or $-y$ direction, to move the IDW toward the upper edge; the sign depends on whether the IDW has a H2H or T2T structure. The resulting $v_{\rm IDW}(B_{\rm ext})$ curves are shown in Fig. 5, separately for the four possible IDW configurations, revealing that for $B_{\rm ext}$ above a small depinning field, the T2T IDWs move significantly faster than the corresponding H2H IDWs. This can be understood by considering the force due to $B_{\rm ext}$ on the IDW (with $\mathbf{m}^{\rm IDW}$ along $\pm x$) in directions perpendicular to the main DW (white arrows in Fig. 4): for H2H IDWs, the force direction coincides with that due to the line tension of the curved main DW [Figs. 4(a) and 4(b)]. Thus, during the dynamics of the IDW, part of the energy of the driving field is dissipated in partial straightening of the main DW, resulting in

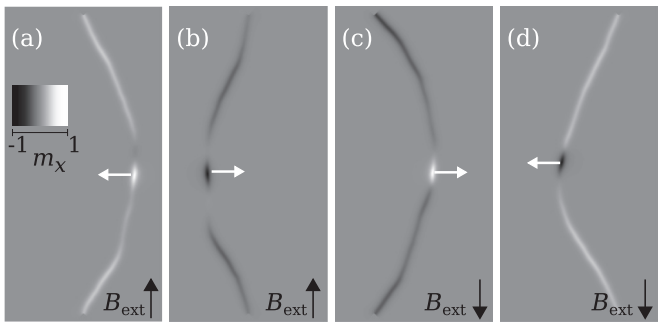

FIG. 4. Snapshots of IDWs of different structures, driven from bottom to top by a field $B_{\rm ext}$ along the $\pm y$ direction, shown as black arrows. The grayscale indicates the magnitude of m_x. IDWs in (a) and (b) are of the H2H type, whereas (c) and (d) have T2T configurations. Depending on the sign of $\mathbf{m}^{\rm IDW}$, $B_{\rm ext}$ gives rise to a force acting on the internal DW either toward left or right, as shown by the white arrows.

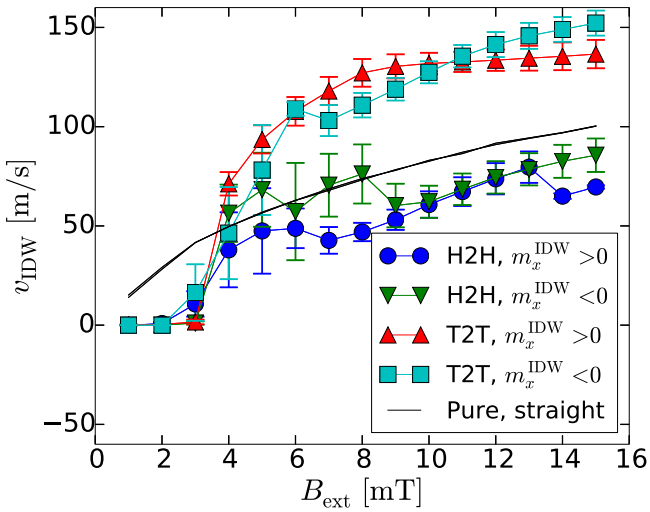

FIG. 5. (Color online) The average (over four disorder realizations) IDW velocity $v_{\rm IDW}$ as a function of $B_{\rm ext}$ for the four possible IDW configurations (see Fig. 4 for the direction of $B_{\rm ext}$ in each case). The black lines show the corresponding data for perfect strips with artificially generated straight main DWs, each containing an IDW of one of the four different kinds (H2T, T2T, $m_x^{\rm IDW} > 0$, $m_x^{\rm IDW} < 0$). For $B_{\rm ext}$ exceeding 15 mT, the domain structure starts to break down.

a lower v_{IDW} for H2H IDWs. For T2T IDWs, the perpendicular force on the IDW due to the driving field points in the opposite direction from that of the curvature-induced force: thus, less motion of the main DW takes place during the IDW dynamics, and a larger fraction of the field energy is available to move the T2T IDW, resulting in a larger v_{IDW}. This is confirmed by movies provided as Supplemental Material [39]: the motion of T2T IDWs is noticeably smoother than that of H2H IDWs. As a further check, we consider also a pure system with an artificially generated straight main DW containing an IDW; the resulting $v_{\mathrm{IDW}}(B_{\mathrm{ext}})$ curves for the four possible configurations are shown as solid black lines in Fig. 5. All cases exhibit the same $v_{\mathrm{IDW}}(B_{\mathrm{ext}})$ behavior, which is intermediate between those found for curved main DWs with H2H and T2T IDWs, respectively. Thus, the perpendicular forces still play a role in energy dissipation, but less than in the curved H2H case.

The $v_{\mathrm{IDW}}(B_{\mathrm{ext}})$ curves in Fig. 5 exhibit two noteworthy features: (i) v_{IDW} grows sub-linearly with B_{ext}, indicating that an increasing fraction of the field energy is dissipated in other processes than IDW motion when B_{ext} is increased. (ii) No clear velocity drop, a signature of Walker breakdown, is observable; this is the case even if we consider relatively large fields up to 15 mT. Inspection of the magnetization dynamics of the IDWs (see Supplemental Material [39]) reveals that the direction of $\mathbf{m}^{\mathrm{IDW}}$ is indeed preserved during the dynamics. This can be understood to follow from the peculiar topology of the system at hand: unlike nanostrips, the main DW along which the IDW is propagating does not have free boundaries; these are crucial, e.g., for nucleation of antivortices, mediating the magnetization reversal of transverse DWs in in-plane nanostrips. Instead, here the IDWs are surrounded by the two out-of-plane domains, which topologically protect $\mathbf{m}^{\mathrm{IDW}}$ from being flipped, leading to the absence of Walker breakdown, and consequently to relatively large field-driven IDW velocities (up to 150 m/s for T2T IDWs). A similar absence of the Walker breakdown of topological origin has been reported in ferromagnetic nanotubes [42].

Finally, we consider current-driven IDW dynamics in narrow perfect CoPtCr strips with the straight main DW located in the middle of the strip and oriented along its long axis (inset of Fig. 6). By extending Eq. (1) with spin-transfer torque terms [43], we observe a simple linear dependence of v_{IDW} on the current density j for $\xi = \alpha$ and $\xi = 2\alpha$ (with ξ the nonadiabatic parameter) up to $v_{\mathrm{IDW}} = 490\,\mathrm{m/s}$ for $\xi = 2\alpha$, whereas for $\xi = 0$, $v_{\mathrm{IDW}} = 0$ for all j (Fig. 6; the same results apply for all IDW types). Thus, Walker breakdown is absent also in current-driven IDW dynamics, due to the topological protection discussed above; this implies also that for $\xi = 0$, IDWs remain intrinsically pinned [44] for any j.

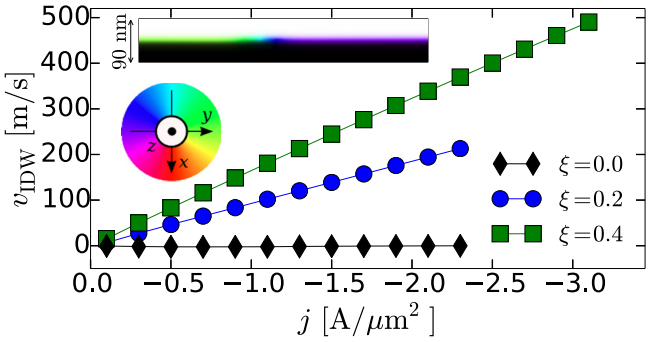

FIG. 6. (Color online) The IDW velocity v_{IDW} as a function of the current density j, for different values of the nonadibatic parameter ξ, in a narrow strip with the main DW along the long axis of the strip; part of such a strip is shown in the inset. For $|j|$ values larger than those shown, the domain structure breaks down.

To conclude, we have shown that for DWs in wide PMA strips, a Walker breakdown-like abrupt reduction of the DW propagation velocity is concurrent with nucleation of internal in-plane domains separated by internal DWs (Bloch lines), resulting in a hierarchical DW structure, with DWs within DWs. The absence of Walker breakdown in the IDW dynamics could lead to interesting possibilities for spintronics applications where DWs would serve as guides for fast IDW propagation.

ACKNOWLEDGMENTS

We thank Mikko J. Alava and Jan Vogel for useful comments. This work has been supported by the Academy of Finland through its Centres of Excellence Programme (2012–2017) under Project No. 251748, and an Academy Research Fellowship (L.L., Project No. 268302). We acknowledge the computational resources provided by the Aalto University School of Science "Science-IT" project, as well as those provided by CSC (Finland).

[1] S. S. Parkin, M. Hayashi, and L. Thomas, Science **320**, 190 (2008).
[2] S. Parkin and S.-H. Yang, Nat. Nanotechnol. **10**, 195 (2015).
[3] D. A. Allwood, G. Xiong, C. Faulkner, D. Atkinson, D. Petit, and R. Cowburn, Science **309**, 1688 (2005).
[4] O. Tchernyshyov and G.-W. Chern, Phys. Rev. Lett. **95**, 197204 (2005).
[5] S. Zapperi, P. Cizeau, G. Durin, and H. E. Stanley, Phys. Rev. B **58**, 6353 (1998).
[6] S. Papanikolaou, F. Bohn, R. L. Sommer, G. Durin, S. Zapperi, and J. P. Sethna, Nat. Phys. **7**, 316 (2011).
[7] V. Lecomte, S. E. Barnes, J.-P. Eckmann, and T. Giamarchi, Phys. Rev. B **80**, 054413 (2009).
[8] F. Garcia-Sanchez, P. Borys, R. Soucaille, J.-P. Adam, R. L. Stamps, and J.-V. Kim, Phys. Rev. Lett. **114**, 247206 (2015).
[9] N. L. Schryer and L. R. Walker, J. Appl. Phys. **45**, 5406 (1974).
[10] E. Martinez, J. Phys. Condens. Matter **24**, 024206 (2012).
[11] E. Martinez, Adv. Cond. Matter. Phys. **2012**, 954196 (2012).
[12] A. Thiaville and Y. Nakatani, in *Spin Dynamics in Confined Magnetic Structures III* (Springer, Berlin, Heidelberg, 2006), pp. 161–205.

[13] J. Żebrowski and A. Sukiennicki, J. Appl. Phys. **52**, 4176 (1981).
[14] J. Leliaert, B. Van de Wiele, J. Vandermeulen, A. Coene, A. Vansteenkiste, L. Laurson, G. Durin, B. Van Waeyenberge, and L. Dupré, Appl. Phys. Lett. **106**, 202401 (2015).
[15] J. Leliaert, B. Van de Wiele, A. Vansteenkiste, L. Laurson, G. Durin, L. Dupré, and B. Van Waeyenberge, J. Appl. Phys. **115**, 233903 (2014).
[16] B. Van de Wiele, L. Laurson, and G. Durin, Phys. Rev. B **86**, 144415 (2012).
[17] Y. Nakatani, A. Thiaville, and J. Miltat, Nat. Mater. **2**, 521 (2003).
[18] H. Min, R. D. McMichael, M. J. Donahue, J. Miltat, and M. D. Stiles, Phys. Rev. Lett. **104**, 217201 (2010).
[19] J. Leliaert, B. Van de Wiele, A. Vansteenkiste, L. Laurson, G. Durin, L. Dupré, and B. Van Waeyenberge, Phys. Rev. B **89**, 064419 (2014).
[20] X. Jiang, L. Thomas, R. Moriya, M. Hayashi, B. Bergman, C. Rettner, and S. S. Parkin, Nat. Commun. **1**, 25 (2010).
[21] V. Volkov and V. Bokov, Phys. Solid State **50**, 199 (2008).
[22] S. Konishi, IEEE Trans. Magn. **19**, 1838 (1983).
[23] A. Malozemoff and J. Slonczewski, Phys. Rev. Lett. **29**, 952 (1972).
[24] J. Slonczewski, J. Appl. Phys. **45**, 2705 (1974).
[25] A. Malozemoff and J. Slonczewski, *Magnetic Domain Walls in Bubble Materials* (Academic Press, San Diego, 1979).
[26] R. Hertel and A. Kákay, J. Magn. Magn. Mater. **379**, 45 (2015).
[27] R. D. McMichael and M. J. Donahue, IEEE Trans. Magn. **33**, 4167 (1997).
[28] Y. Nakatani, A. Thiaville, and J. Miltat, J. Magn. Magn. Mater. **290-291**, 750 (2005).
[29] V. Estévez and L. Laurson, Phys. Rev. B **91**, 054407 (2015).
[30] A. Vansteenkiste, http://mumax.github.io.
[31] A. Vansteenkiste and B. Van de Wiele, J. Magn. Magn. Mater. **323**, 2585 (2011).
[32] A. Vansteenkiste, J. Leliaert, M. Dvornik, M. Helsen, F. Garcia-Sanchez, and B. Van Waeyenberge, AIP Adv. **4**, 107133 (2014).
[33] T. L. Gilbert, IEEE Trans. Magn. **40**, 3443 (2004).
[34] W. F. Brown, *Micromagnetics*, Vol. 18 (Interscience Publishers, New York, 1963).
[35] Y. Kubota, L. Folks, and E. E. Marinero, J. Appl. Phys. **84**, 6202 (1998).
[36] D. Weller, A. Moser, L. Folks, M. E. Best, W. Lee, M. F. Toney, M. Schwickert, J.-U. Thiele, and M. F. Doerner, IEEE Trans. Magn. **36**, 10 (2000).
[37] O. Boulle, S. Rohart, L. D. Buda-Prejbeanu, E. Jué, I. M. Miron, S. Pizzini, J. Vogel, G. Gaudin, and A. Thiaville, Phys. Rev. Lett. **111**, 217203 (2013).
[38] A. K. Zvezdin, A. F. Popkov, and I. P. Yarema, Zh. Eksp. Teor. Fiz. **98**, 1070 (1990) [Sov. Phys. JETP **71**, 597 (1990)].
[39] See Supplemental Material at http://link.aps.org/supplemental/10.1103/PhysRevB.92.100405 for movies illustrating the details of the domain wall dynamics discussed in the paper.
[40] J. Iwasaki and N. Nagaosa, J. Phys. Soc. Jpn. **84**, 083701 (2015).
[41] We expect other sources of disorder, leading to a random energy landscape interacting with the DW, to give rise to similar results.
[42] M. Yan, C. Andreas, A. Kákay, F. García-Sánchez, and R. Hertel, Appl. Phys. Lett. **99**, 122505 (2011).
[43] S. Zhang and Z. Li, Phys. Rev. Lett. **93**, 127204 (2004).
[44] T. Koyama, D. Chiba, K. Ueda, K. Kondou, H. Tanigawa, S. Fukami, T. Suzuki, N. Ohshima, N. Ishiwata, Y. Nakatani *et al.*, Nat. Mater. **10**, 194 (2011).